Int J Adv Manuf Technol
DOI 10.1007/s00170-011-3332-4

ORIGINAL ARTICLE

# On-line 3-D system for the inspection of deformable parts

**Andrés Eleazar Jaramillo · Pierre Boulanger · Flavio Prieto**

Received: 27 December 2010 / Accepted: 5 April 2011


**Abstract** In spite of the development of automated tolerance inspection systems for manufactured parts over the years, there are still processes that inevitably require manual intervention making full automation impossible in most cases; in particular when dealing with deformable parts. In most current industrial inspection systems, a deformable part under inspection must first be mechanically constrained on a rigid support or jig so as to be able to compare it with its nominal shape. This paper presents a new system to perform real-time surface inspection of deformable parts that does not require fixturing. Instead, the proposed system applies virtual forces to the part's CAD model as if the part was installed in the fixturing device. Normally, a precise finite element method (FEM) simulation should be used to approximate the deformation that appends when the part is installed in the device. Even with a fast parallel computer, FEM is far from being real-time and cannot be used for on-line inspection. In the proposed system, a radial basis function approximation of the FEM simulation is trained off-line and used to speed-up the simulation by an order of magnitude. Experimental evaluation of the proposed system is presented for three plastic parts. Using the proposed scheme, an approximation of 0.25 mm compared with the real deformation was obtained. In this paper, statistical results are presented such as the average deviation, standard deviation, and processing time between the approximations obtained with the proposed method and with the finite element method applied to the full CAD model.

**Keywords** Deformable parts · 3-D inspection · Radial basis functions · Nonrigid registration · On-line inspection

A. E. Jaramillo (✉)
Universidad Nacional de Colombia,
Cra 27 No. 64-60 Manizales, Caldas, Colombia
e-mail: aejaramillov@unal.edu.co

P. Boulanger
University of Alberta, Athabasca Hall, Room 411,
Edmonton, Alberta, T6G 2E8, Canada
e-mail: pierreb@ualberta.ca

F. Prieto
Universidad Nacional de Colombia, Carrera 30 No. 45-03,
Edif. 453—Of. 404, Bogotá, Colombia
e-mail: faprietoo@unal.edu.co

## 1 Introduction

Inspection of manufactured parts is an essential factor in today's competitive industries, such as automotive and aerospace, where high-quality products are required [1]. In these industries, there are already measuring systems such as coordinate measuring machines, photogrammetry systems, and laser probes, which can perform inspection tasks at high speed and high precision (better than 25 μm) [2–4]. However, many of those systems are typically large and bulky and cannot be installed easily at the production line [5]. This limits the dimensional inspection system to assessing tolerances off-line on samples taken randomly from a batch of parts [6].

Traditionally, the inspection of three-dimensional (3-D) parts is done by performing a comparison between a reference model, or CAD model, and the measurements of the part's surface by a 3-D sensor. The part to be inspected is mounted into a jig and reference points are measured to determine the rigid

Published online: 04 May 2011

transformation between the CAD model and the part [7]. Following this registration, the measuring system then acquires key points, in order to evaluate if the part is in tolerance relative to the specifications defined in advance by designers. Some of these tasks are manual and difficult to automate. There have been many attempts to perform inspection automatically. Under some conditions, those systems could do automatic dimensional validation [8, 9]. However, due to the development of new materials as well as more complex structural shapes, many parts are remarkably flexible. In these cases, it is necessary to carry out a fixturing process using a jig to fix the part to its nominal shape. As with traditional inspection, this fixturing process is time consuming and difficult to automate.

This paper presents a new system to perform real-time surface inspection of deformable parts that does not require fixturing. Instead, the proposed system applies to the part's CAD model virtual forces as if the part was installed in the fixturing device. Normally a precise finite element method (FEM) simulation should be used to approximate the deformation that appends when the part is installed in the fixturing device. Even with a fast parallel computer, FEM is far from being real-time and cannot be used for on-line inspection. In the proposed system, a radial basis function (RBF) approximation of the FEM simulation is trained off-line. In the training stage, deformations are simulated by a precise FEM. Using these reference deformations, a minimum set of control points is calculated approximating the FEM deformation model by RBF interpolation, to approximate the deformation of the CAD model under constraints. After the nonrigid alignment between the CAD model and the part data, a comparison is carried out and a tolerance evaluation report is generated.

The paper is organized as follows. The next section reviews related work. Section 3 briefly presents the theoretical foundations involved in the proposed approach. Section 4 describes the proposed system. Section 5 presents various tests with industrial parts and analyzes the results. Finally, we conclude and indicate future research directions.

## 2 Literature review

Numerous research has been published in the literature relating to the development of new methods and systems for the automation of part inspection. Some of these works focus on specific inspection processes. Suh et al. introduced a system for assessing the main features of spiral bevel gears: tooth profile, tooth trace, and pitch errors [10]. Thomas et al. developed a system to detect defects in hardwood logs and stems [11]. Shao et al. presented an inspection system for parts with large areas, especially large sheet-metal pieces like those for stamping for use in the automotive and aerospace industries [12].

However, most of the research efforts in dimensional inspection is devoted not to quality evaluation of specific products, but rather to avoid steps performed by human operators, or to develop integrated systems that would allow the user to control the whole inspection process. Germani et al. developed such an integrated inspection system that permits the designer to define the tolerances and supervise the inspection process, from the planning phase to the tolerance verification, using a specialized software environment [13]. This system includes a full information database of the part design, an articulated robot system, and 3-D scanners. The aim of that work is to connect the design stage with the quality control process to reduce time and cost associated with the inspection process. Rodrigues et al. presented a system devoted specifically to automate the measurement planning stage of a part [14]. They propose a method to optimize the number of views and paths for the movement of the acquisition system based on information provided by the part's CAD model.

The process of registration or alignment of the part's CAD model with the measurements data is the most important stage in the 3-D inspection. This is the subject of the work presented by Ravishankar et al. in [15]. The paper describes a fast algorithm to automate CAD-data comparison for the inspection of curves and surfaces like the one found in aerospace. The proposed registration method is based on the well-known iterative closest point (ICP) algorithm to automate the alignment step in the inspection process. Shi and Xi also present a method based on ICP algorithm to automate registration of views during the inspection of industrial parts [16]. An algorithm to remove outliers so as to preserve surface details was developed and used in a multi-view registration process.

Some researchers have presented works which can deal with deformable parts. Zhang et al. presented a photogrammetric method to measure deformation of flexible sheet-metal parts [17]. Kim proposed a measurement system to calculate deformation and misalignment of deformable peg-hole pairs to be assembled [18]. Merkley et al. proposed a method to perform tolerance analysis in the assembly of deformable parts [19].

However, to our knowledge, only Weckenmann et al. have presented a system devoted to the automation

of deformable parts inspection process [20, 21], which has been recently validated by Lemes [22]. In Weckenmann's work, a 3-D inspection system for sheet-metal parts is proposed. The system uses a triangulation-based 3-D sensor to measure the part's surfaces. From these measurements, a smoothed and optimized triangular mesh of a part's visible surface is generated. Then the system applies virtual forces to a FEM representation of the part model create from the measured data to compensate for its deformation. This method requires taking data from the entire deformed surface in order for the simulation to be accurate. This is not ideal as it is rare that one can capture all the surface elements of a complex part because of occlusions and sensor access.

From this short review, one can conclude that automation of parts surface inspection is still an open field of research, in particular when the inspected parts are deformable in its assembly stage. In this paper, we explore a novel way to automate the inspection process by speeding up the computation of the deformations involved in the alignment of virtual models with the measured data. Preliminary ideas of this work were presented in [23].

## 3 Surface inspection of deformable parts

The proposed system needs some theoretical elements that are not present in traditional inspection systems. This section briefly presents the mathematical foundations of the most important elements. The general scheme applied to industrial inspection of parts is also reviewed.

### 3.1 Three-dimensional surface inspection of parts

In general, one can define the inspection process as a measurement on how a part or a product deviates from its given set of specifications [24]. In particular, when one deals with 3-D surface inspection of parts, specifications may refer to some surface features, such as flatness, roundness, etc., or in general, to the whole shape of the part.

In order to get more flexibility in industrial inspection systems, a scheme based on the CAD model of the parts to inspect is used so that they can be applied to parts of different shapes. This scheme is composed of the following stages (Fig. 1):

1. A 3-D data acquisition process where the part surface is measured by a 3-D sensor. This stage includes the measurement system, the data processing, and the construction of a polygonal model from the measured data.
2. A data alignment process where the 3-D measurements and the part's CAD model are registered. The alignment process is performed by computing a rigid transformation to establish a common reference system for the CAD model and the part measurements. The transformation is calculated iteratively on the entire part's surface from a set of corresponding points between the two models.
3. A comparison process where the deviations from the measurements relative to the CAD model are calculated. The results allow us to determine whether or not the part meets the required specifications.

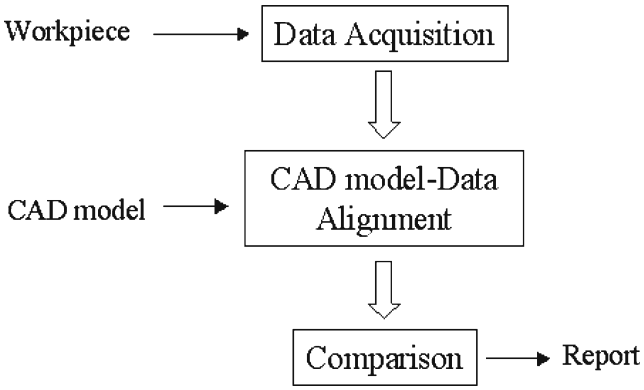


**Fig. 1** Basic steps in CAD-based inspection

### 3.2 Alignment of deformable models

The method described in the previous section assumes that the inspected parts did not change their shapes when they were measured. Therefore, a rigid transformation is enough to align the measurements from the inspected part with its CAD model. However, there are many parts that only acquire their final shapes when they are assembled. In those cases, to perform validation of a part using the current inspection system, it is necessary to manually fix them on a mechanical device prior to data acquisition. This paper proposes a new approach where, instead of applying a true deformation to the inspected part, a virtual deformation is applied on the CAD model during the model alignment stage (Fig. 2). In order to simulate a real-physical deformation, a FEM is used for the calculation of the physical deformation, and RBFs are used to approximate the deformation and to reduce the computational burden to perform the nonrigid deformation on-line.

A general expression for the required nonrigid transformation consists of a linear term, corresponding to a

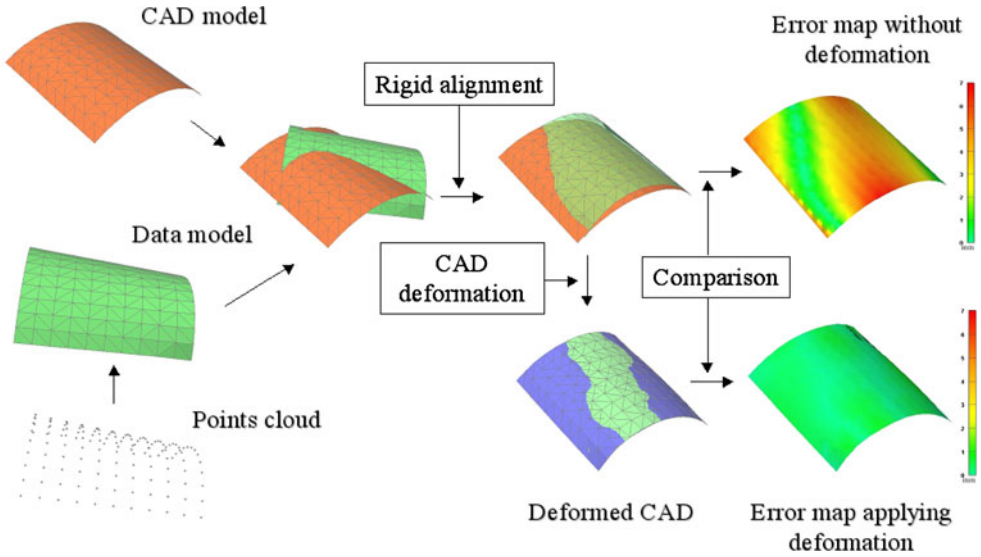


**Fig. 2** Alignment and evaluation of a deformable model

rigid transformation, and a nonlinear term corresponding to a deformation. Let $\mathbf{P} = \{\mathbf{p}_i\}$, with $i = 1, ..., n$, be a set of points representing a given model, the overall transformation $\mathbf{F}$ applied to this set of points can be written as:

$$\mathbf{F}(\mathbf{p}_i) = \mathbf{U}(\mathbf{p}_i) + \mathbf{M}\mathbf{p}_i + \mathbf{t} \tag{1}$$

where $\mathbf{U}(\cdot)$ is a nonlinear transformation, $\mathbf{M}$ is a rotation matrix and $\mathbf{t}$ is a translation vector. The first term represents the deformation and the others represent the rigid transformation.

Since a rigid transformation is applied before aligning the models, only the deformation term is necessary at this stage. The translation vector is set to zero and the rotation matrix is the identity matrix, so Eq. 1 is simplified to:

$$\mathbf{F}(\mathbf{p}_i) = \mathbf{U}(\mathbf{p}_i) + \mathbf{p}_i \tag{2}$$

### 3.3 Physics-based deformation

Finite element methods are critical tools for the analysis of stress and deformation in structures [25, 26]. In order to use FEM, the part's CAD model is divided into a set of continuous computing units called elements, for which it is possible to generate simple functions that describe their behavior under stress with great precision. For the sake of simplicity, the elements are basic geometric shapes such as quads, triangles, and tetrahedrons, etc., which are linked together to form a 3-D mesh. FEM programs need to solve a set of equations that represent continuous mechanics laws between elements and their set boundary conditions.

We assume that the deformation law of the part material can be solved by a simple shell element method. A shell element can be defined as a thin body bounded by two surfaces separated by a small distance. If the bounding surfaces are not closed, then the shell has edges and the distance between such edges is normally large compared with their thickness. When an external force is applied to a shell structure, mainly two types of internal forces are produced: membrane forces and bending forces. Membrane forces act tangentially to the mid-plane of the element; therefore, axial forces and membrane shear forces are part of this type of internal force. On the other hand, flexing, twisting, and transverse shear are bending forces. The Mindlin–Reissner formulation for thick shell elements was chosen for our simulations [27]. This is a more general formulation of shell elements than the classical Kirchhoff plate and more appropriate to simulate deformation of plastic and stamping parts.

### 3.4 Radial basis functions

A radial basis function is a real-valued function whose value depends only on the distance to a reference point called the center or the control point [28]. Although different distance functions are possible, Euclidean distance is usually used. A property of these functions is that they form a basis, that is, any function that can be approximated by a linear combination of RBFs. For our purposes, linear combinations of RBFs are used to approximate the final shapes of the deformed part's model.

Given a set of control points $\mathbf{q}_j$, with $j = 1, ..., m$, take from a full set of points $\mathbf{P}$ and a distance function

$d(\cdot)$. The nonlinear transformation $\mathbf{U}(\cdot)$ obtained as the linear combination of the RBFs is written as:

$$\mathbf{U}(\mathbf{p}_i) = \sum_j \mathbf{C}_j R(d(\mathbf{p}_i, \mathbf{q}_j)), \tag{3}$$

where $\mathbf{C}_j$ is the weight vector associated to each center $\mathbf{q}_j$, and $R$ represent the basis function. For this study, multi-quadrics basis functions $R(d) = (d^2 + \beta^2)^{1/2}$ were used. These functions are time-efficient RBFs [29]. The $\beta$ parameter for each center $\mathbf{q}_j$ is computed from the minimum distance to the other centers $\mathbf{q}_k$ [30]:

$$\beta_j = \min_{j \neq k} d_j(\mathbf{q}_k). \tag{4}$$

Other RBFs such as Gaussian $R(d) = e^{-(d/\beta)^2}$ as well as the inverse multi-quadrics $R(d) = 1/(d^2 + \beta^2)^{1/2}$ have been tested, but no significant advantages have been found [31].

Since we are only interested at modeling the deformation, an additional term is considered in the transformation. This term allows us to recover the original form in the case where there is no movement of the control points. According to Eq. 2, the transformation required to be applied to the set $\mathbf{P} = \{\mathbf{p}_i\}$, with $i = 1, ..., n$, can be written as:

$$\mathbf{F}(\mathbf{p}_i) = \sum_j \mathbf{C}_j R(d(\mathbf{p}_i, \mathbf{q}_j)) + \mathbf{p}_i. \tag{5}$$

In the calculation, the input domain is the set of nodes of the CAD mesh, and the transformation $\mathbf{C}_j$ weights are determined by the specific displacements of the control points.

## 4 Representation of FEM deformations using RBFs

As in CAD-based inspection systems, the proposed system is based on the comparison of 3-D surface data measurements taken from a part against its CAD model. But, unlike traditional systems, in addition to the rigid transformation a deformation is applied to align the CAD model to the measured data. Both, rigid and nonrigid transformations use correspondences between clamping points (specified in advance) in the CAD model and the data set. This section describes the general approach and the main ideas behind this work.

### 4.1 Inspection system

The proposed approach consists of two main steps. One can see in Fig. 3 an overview of the inspection system. In the first stage, prior to the tolerance inspection, a training process is carried out. At this stage, from the CAD model and material properties of the part, the minimum number of control points of the full CAD mesh is determined. This set of control points allows us to approximate the FEM simulated deformation within a certain error level using RBF interpolation. Then, a simplified polygonal mesh of the part is built using the minimum set of control points.

In the second stage, the evaluation process of the inspected part is performed. The process begins with the acquisition of 3-D measurements from the surface of the part under inspection. The system only required that the part is located in the acquisition space of the sensor and does not need to be fixed on a jig. Contrary

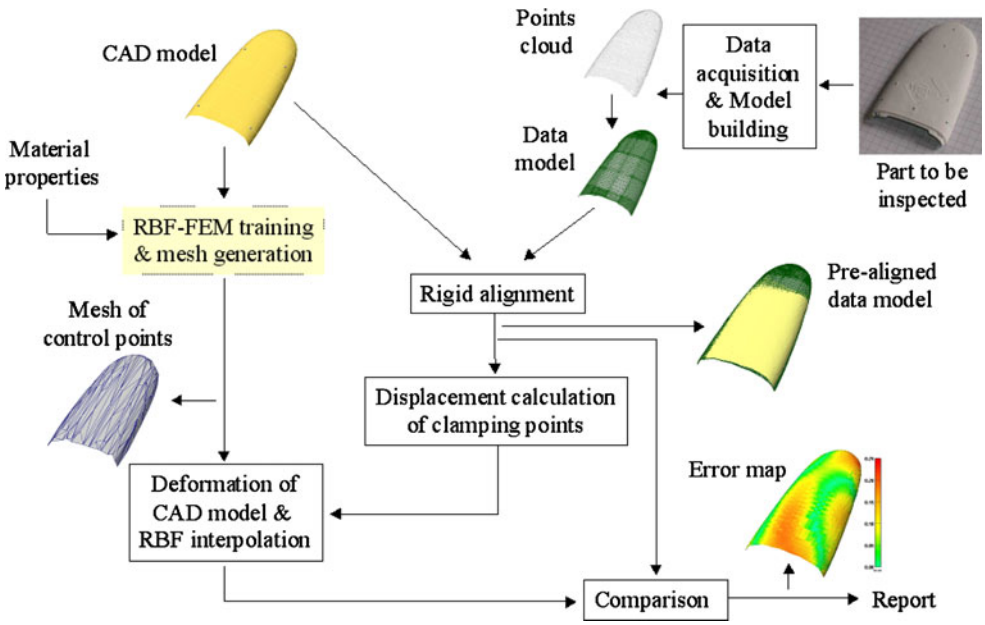


**Fig. 3** Overview of the inspection system

to the work of Weckenmann et al. [21], although, a polygonal model from the measured data is built for validation purposes, this step is not necessary since only a rigid transformation and not deformation is applied on the measured data. The rigid transformation is carried out by taking into account the correspondences of clamping points between the CAD model and the measured data. Once the alignment is performed, the deformation of the reduced mesh obtained in the training stage is calculated. The displacements of the clamping points are taken as constraints for the FEM calculation of deformation. Then, the interpolation with RBFs is performed on the resulting deformed mesh to get the full set-of-points representing the deformed CAD model. In this way, the nonrigid alignment between the CAD model and measurement data is obtained.

Finally, the calculation of the deviations of the deformed CAD model to the measured data is carried out and a final tolerance report is generated. This report indicates the acceptance or rejection of the part according to a predefined set of criteria. The closest distance to the deformed CAD model was taken for the calculation of deviations of the measured data, and as a criterion for acceptance, it was established that a part is in tolerance if 95% of all measured points are within the chosen tolerance.

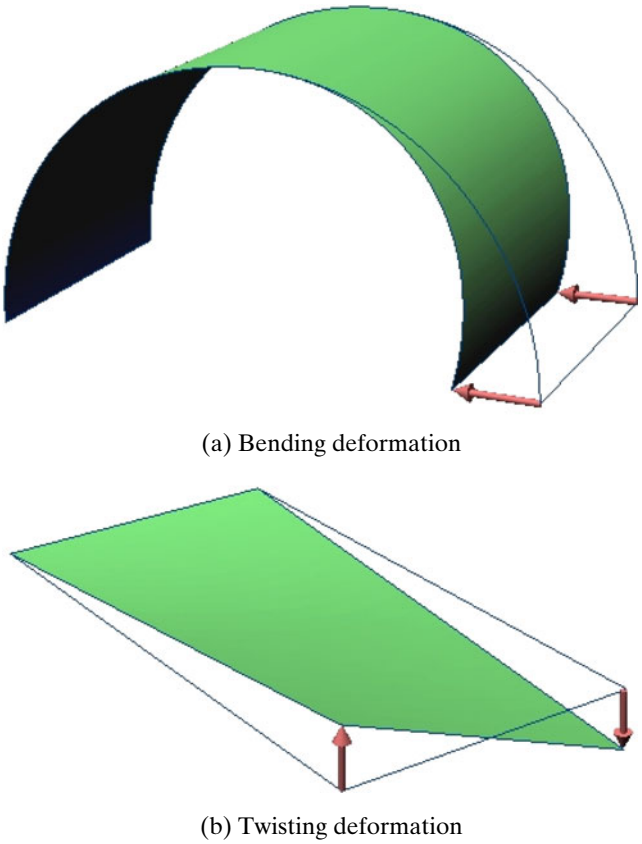

(a) Bending deformation

(b) Twisting deformation

**Fig. 5** Deformations applied during the training process

## 4.2 RBF deformation training

It was experimentally observed that the effect of the tangential forces acting on the parts is not important. Then, only displacements due to the normal forces are considered in the training stage (Fig. 4). That is, membrane behavior is neglected and only flexing and twisting behaviors are taken into account in the RBF training process (Fig. 5). In this way, only displacements and not the moments of rotation of the clamping points, are considered.

The bending deformations are simulated using FEM analysis. Force loads and constraints applied in the training stage are chosen based on the knowledge and handling of a real part. The forces are applied to the clamping points of the part. Directions are chosen in such a way that bending and twisting deformations are produced (see Fig. 5). Force magnitudes are set to produce small displacements in order to respect the fact that we are using linear FEM.

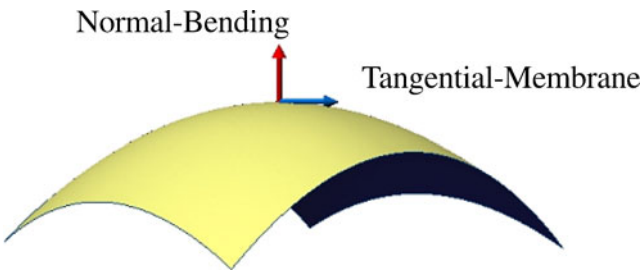


**Fig. 4** Normal and tangential forces on a 3-D surface

## 4.3 Iterative approach to error minimization

This is an off-line process. The goal of this process is to determine a minimal set of points from the full CAD mesh that will allow us to approximate the deformation model using RBF interpolation. The quality of the approximation is evaluated according to a maximum acceptable deviation threshold $\delta$ defined by the user. Training deformations provided by FEM simulation are then used as reference deformation models.

The minimal set of center points for the RBF interpolation is computed using an iterative algorithm (Algorithm 1). The initial set corresponds to the clamping points locations. At each step the interpolation with RBFs is performed (see Eq. 5). Then, deviation between each node $i$ from the training mesh $\mathbf{p}_t$ and its equivalent vertex in the CAD mesh $\mathbf{p}_a$, is computed.

If the maximum deviation $E_{i\_max}$ exceeds the threshold $\delta$, then the corresponding node is added to the set of control points and the RBF interpolation is performed again. This iterative process will stop when the maximum deviation is smaller than the threshold defined by the user or when the number of control points is bigger than a predefined maximum number of control points **Q**. In order to guarantee an important reduction in the number of control points relative to the FEM analysis, **Q** was set to be only 10% of the total number of nodes in the CAD mesh. For the three parts, Table 2 shows the total number of nodes (first row) and the number of control points (second row) at the end of the iterative process. This result shows that the algorithm converges before reaching the maximum number of control points.

**Algorithm 1** Computation of a minimal set of control points

**Require: Input data:**
$\mathbf{p}_a$ : vertex from CAD mesh.
$\mathbf{p}_t$ : nodes from training deformed mesh.
$\mathbf{c}_a$ : clamp the points.
$\delta$ : maximum deviation threshold.
**Q** : maximum number of control points.
**Step 1.** Set control points $\mathbf{q} = \mathbf{c}_a$.
**Step 2.** Compute the RBF interpolated points $\mathbf{p}_b$, using $\mathbf{p}_a$ as input points and **q** as centers.
**Step 3.** Calculate deviation for each node $i$, $E_i = |\mathbf{p}_{bi} - \mathbf{p}_{ti}|$, and find the maximum, $E_{i\_\max}$.
**Step 4. IF** $E_{i\_\max} > \delta$ **AND** the number of nodes in **q** $<$ **Q THEN** add $\mathbf{p}_{i\_\max}$ node to the set **q**.
**Step 5. IF** $E_{i\_\max} > \delta$ return to Step 2.
**Output**: **q**, the minimum set of control points.

### 4.4 Simplified mesh

Since FEM simulation requires connectivity between the nodes, a simplified mesh of the part model is generated from the final set of control points obtained in the previous stage. This simplified mesh is deformed using FEM analysis. This way, a lighter physical model is provided to the CAD model deformation process. Constraints to solve the FEM problem are generated by the displacements applied to the clamping points on the simplified mesh to the corresponding points on the measured data (Fig. 6).

### 4.5 Deformation calculation

This stage adds deformation to the alignment process when the inspection of the part is carried out. In the proposed approach, the CAD model is deformed instead of the data model. The result is the required nonrigid alignment between the CAD model and the data model of the part. This process is summarized in Algorithm 2.

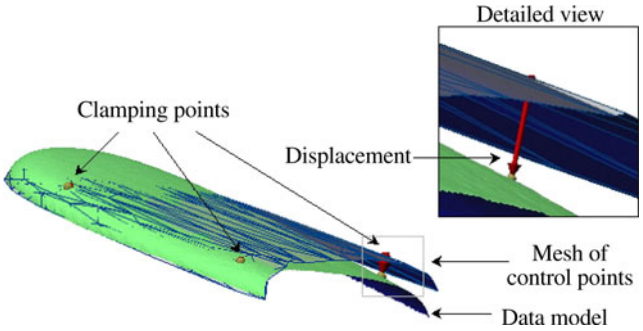


**Fig. 6** Constraints imposed to solve the FEM problem

**Algorithm 2** On-line deformation

**Require: Input data:**
$\mathbf{p}_a$ : vertex from CAD mesh.
$\mathbf{c}_a$ : clamping points on CAD model.
$\mathbf{M}_q$ : mesh of control points.
**w** : data from the part.
**Step 1.** Detect clamping points on data model, $\mathbf{c}_w$.
**Step 2.** Apply a rigid transformation to align **w** to $\mathbf{p}_a$ using $\mathbf{c}_a$ and $\mathbf{c}_w$ correspondences.
**Step 3.** Compute displacements between corresponding clamping points, $\mathbf{d}_i = \mathbf{c}_{wi} - \mathbf{c}_{ai}$.
**Step 4.** Apply **d** to deform $\mathbf{M}_q$ using FEM.
**Step 5.** Interpolate deformed $\mathbf{M}_q$ using RBFs to get the approximated deformed CAD $\mathbf{p}_x$.
**Output**: $\mathbf{p}_x$, the set of nodes of approximate deformed CAD.

In order to identify node coordinates of the clamping points on the measured data, a hole detection algorithm can be applied [32, 33]. Then, given the corresponding coordinates of the clamping points on the measured data and the CAD model, a pre-alignment is carried out. The pre-alignment consists of a rigid transformation defined by a rotation and a translation.

In the inspection process, displacements from the clamping points in the CAD model to corresponding points in the pre-aligned data model are computed. Instead of applying forces, these displacements are used as loads and constraints in the FEM analysis, and are applied to the mesh of control points. This way, a physical deformation is considered in the nonrigid alignment. Although force magnitudes are not known beforehand (because they are not necessary) they could be computed in the FEM analysis if needed.

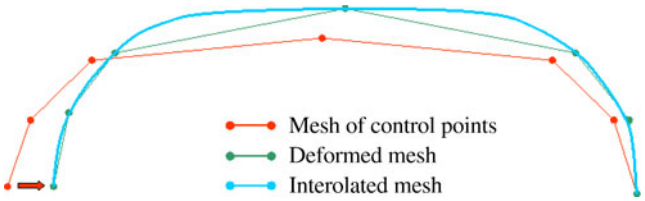


**Fig. 7** Deformation and interpolation on a polygonal curve

Finally, using the deformed control points obtained from the FEM simulation, the RBF interpolation is used to approximate the deformation. This time, the full set-of-points of the CAD mesh is the input and the set of control points is the set of RBF centers. The result from interpolation is the deformed set-of-points of the CAD model needed to align the CAD model with the measurement data. Figure 7 shows an example of the deformation and interpolation process on a polygonal curve.

## 5 Results

Tests were performed using a 2.16 GHz Intel dual core processor with 2GB RAM, running a Microsoft Windows XP operating system. FEM simulations were performed using SAP2000 [34], and RBF-FEM algorithms were implemented using MATLAB. Three-dimensional data points were acquired with a Minolta Vivid 9i laser scanner. Figure 8 shows the experimental setup.

The system was tested on three plastic parts. The material properties and dimensions of the models for the FEM calculations were the following: Young's modulus of elasticity = 25,000 kgf/cm$^2$; Poisson's ratio = 0.35; thickness = 0.2 cm for part 1 and 0.4 cm for parts 2 and 3. The dimensions of the bounding box are summarized in Table 1.

Due to the shell structure of the parts and the bending forces applied, thickness is the parameter that most affects the flexibility of the part and the results of the FEM simulations [35]. The bending stiffness $D$ of a plate with thickness $h$ is expressed by $D = Eh^3/(12(1-\nu^2))$, where $E$ is the Young modulus and $\nu$ is the Poisson's ratio of the material. For this reason, changes in thickness produce changes in the shape of the deformation computed by the FEM calculations. As a first approximation, this parameter was assumed constant. There is no doubt that in order to improve accuracy, a variable thickness should be considered to define the appropriate thickness for each shell element of the FEM model. In order to solve this problem one could also use volume elements instead but at the expense of long calculations.

**Fig. 8** Experimental setup

Figures 9a, d, and g show the nonrigid alignment for the models of parts 1, 2, and 3, respectively. In each case, one can see the undeformed CAD model in red, the measured data in green, and the approximate deformation obtained with the proposed method in blue. The red arrows indicate the feature point where displacement to deform the models was applied. Figure 9b, e, and h show the cross-sections generated by the plane indicated in the previous figures. From these figures, one can see that the approximate deformation improves the alignment between the undeformed CAD model and the data model of the deformed part. Figure 9c, f, and i show the error map in pseudo-color that indicates the absolute deviation of the RBF-FEM approximation for a real deformation. The shortest distance from point to surface was used to calculate the distances between

**Table 1** Bounding box dimensions of the parts

| Part | $x$ (mm) | $y$ (mm) | $z$ (mm) |
|---|---|---|---|
| 1 | 49.73 | 85.62 | 12.92 |
| 2 | 206.20 | 225.46 | 76.57 |
| 3 | 155.67 | 157.90 | 37.82 |

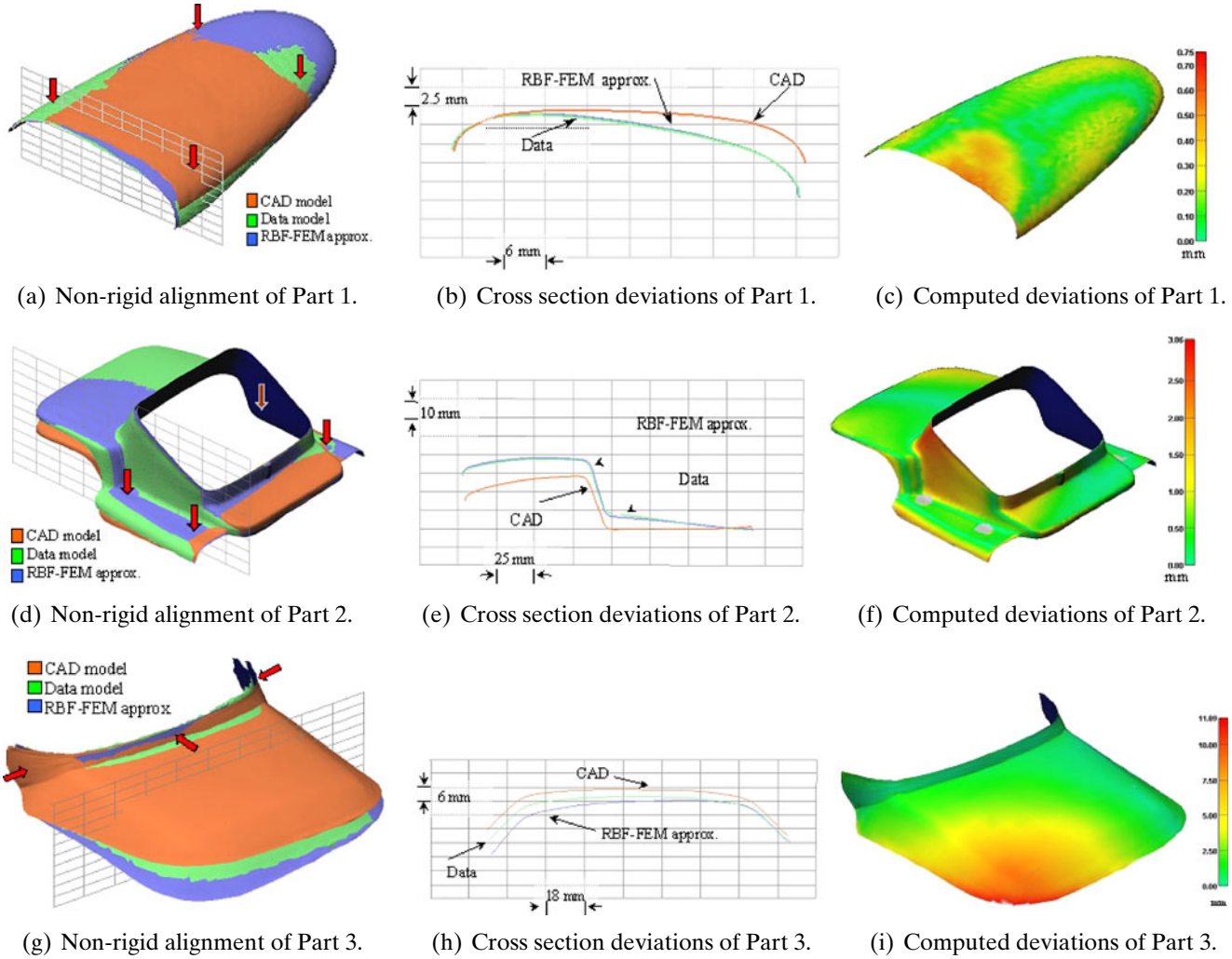


(a) Non-rigid alignment of Part 1. (b) Cross section deviations of Part 1. (c) Computed deviations of Part 1.

(d) Non-rigid alignment of Part 2. (e) Cross section deviations of Part 2. (f) Computed deviations of Part 2.

(g) Non-rigid alignment of Part 3. (h) Cross section deviations of Part 3. (i) Computed deviations of Part 3.

**Fig. 9** Inspection of real deformed parts

the nodes of the approximate deformed CAD model and the polygonal model created from the measured data points. The error display was adjusted to use the full scale of the color map. Gray points were not taken into account in the calculations. These regions are seen especially in Fig. 9f around the points where the forces were applied and at the edge of the model.

Table 2 provides a summary of the numerical results for each part.

The number of nodes and the number of control points indicates the total number of nodes used in the CAD model, and the number of control points used to approximate the real deformation, respectively. The last one was computed using Algorithm 1.

The maximum distance value is set beforehand by the user. So, points beyond that limit are not taken into account in the calculations. The table also presents maximum deviation values, estimates of average, standard deviations, and the percentages of points within ±1, ±2, and ±3 standard deviations. Deviations are positive if the approximate deformed model is over the reference, and otherwise they are negative.

**Table 2** Comparison of RBF-FEM approximation related to data model

| | Part 1 | Part 2 | Part 3 |
|---|---|---|---|
| Number of nodes | 3,826 | 18,986 | 2,711 |
| Number of control points | 151 | 104 | 42 |
| Max. distance value (mm) | 2.00 | 4.00 | 12.00 |
| Max. deviation positive (mm) | 1.06 | 3.94 | 2.85 |
| Max. deviation negative (mm) | −1.04 | −3.93 | −11.89 |
| Average deviation (mm) | 0.06 | 0.15 | −1.154 |
| Standard deviation (mm) | 0.24 | 0.97 | 2.88 |
| % Pts within ± 1 SD | 69.21 | 73.92 | 81.59 |
| % Pts within ± 2 SD | 96.39 | 93.47 | 92.18 |
| % Pts within ± 3 SD | 99.24 | 99.48 | 98.52 |
| Geometric tolerance (mm) | ±1.00 | ±2.00 | ±2.00 |
| % Pts in tolerance | 99.87 | 94.16 | 76.54 |
| Pass/fail | Pass | Fail | Fail |

**Table 3** Comparison of FEM vs RBF-FEM approach

| | Part 1 | | Part 2 | | Part 3 | |
|---|---|---|---|---|---|---|
| | FEM | RBF-FEM | FEM | RBF-FEM | FEM | RBF-FEM |
| RMS deviation (mm) | 0.19 | 0.25 | 0.75 | 0.99 | 4.27 | 3.10 |
| Computation time (s) | 82.448 | 0.022 | 1513.785 | 0.009 | 27.469 | 0.003 |

The geometric tolerance (GT) is the maximum allowable deviation from the nominal value (NV), set according to manufacturing requirements, to determine if the part is to be accepted or rejected. That is, geometric tolerance is the maximum permissible interval where the geometry of the part under control, in its assembly stage, can vary. The interval is measured from the nominal value, in this work the central value of the deformed model, and is defined as: [NV−GT,NV+GT]. The geometric tolerance is set to be half of the thickness of the part, to guarantee that the deviation is not bigger than the thickness of the part. However, this geometric tolerance is usually set by the designer of the part and is determined by functional analysis. A point is said to be in tolerance if its distance to the nominal value is smaller than the geometric tolerance, or in our case, smaller than half of the thickness. To control or inspect a part, the following rule is set as an acceptance criteria. A part is accepted to be in tolerance if at least 95% of points are in tolerance that is, if the distance for at least 95% of points falls below the geometric tolerance. Otherwise it is rejected. The last line of Table 2 indicates the acceptance or rejection of a part according to this criterion.

Table 3 shows a comparison between FEM full mesh calculation and the RBF-FEM approximation. A data model was taken as reference to calculate deviations. Root mean square deviations and times for solving equations are presented for both methods. This comparison shows that for parts 1 and 2, the FEM simulation better approximates the physical deformation while for part 3, the simulation done with the proposed method produces a better approximation. Table 3 also shows that in all cases the processing time is reduced by an order of magnitude using our algorithm, allowing for real-time control.

## 6 Conclusions

This paper presents a new system for surface inspection of deformable 3-D parts. The proposed system is based on the comparison of surface measurements taken from a part against its CAD model. Unlike traditional inspection techniques where it is necessary to fix the deformable part in a jig before performing the measurements, a virtual fixturing process is used to generate virtual deformations on the CAD model. Contrary to normal CAD-based inspection systems, data acquisition is performed on the unconstrained part where an approximate rigid and nonrigid registration is performed based on the displacements of corresponding clamping points between the CAD model and the data model. Since the required transformation corresponds to a physical deformation, an FEM is applied to calculate the deformation but is not really real time. We have demonstrated that by using an RBF approximation one can increase the inspection speed by order of magnitude on a conventional computer opening the door to real-time inspection.

Although the approximation obtained by the proposed RBF-FEM system is not as accurate as the full FEM simulation, because of the order of magnitude speed-up of the RBF method, the approximation error could be set to an acceptable level that is below the GT of the part during its training phase.

In addition, in the proposed approach the deformation is applied to the CAD model as opposed to the measured data. Because only the positions of the corresponding clamping points are required to calculate the deformation, it is not necessary to digitize the entire part surface but only regions to be inspected as well as the surrounding the clamping points. In the future, we are planning to explore the possibility of performing a nonrigid registration process without the specific knowledge of the part fixation point positions by adding more constraints and rapidly exploring the solution space using fast parallel processors like the GPUs.

## References


1. Bogue R (2008) Car manufacturer uses novel laser scanner to reduce time to production. Assem Autom 28(2):113–114
2. Mitutoyo American Corporation. http://www.mitutoyo.com. Accessed 01 April 2011
3. Geodetic Systems Inc. http://www.geodetic.com. Accessed 01 April 2011
4. Faro Technologies Inc. http://www.faro.com/usa.aspx. Accessed 01 April 2011
5. Mears L, Roth J, Djurdjanovic D (2009) Quality and inspection of machining operations: CMM integration to the machine tool. J Manuf Sci Eng 131(5):051006

6. Lee S, Chang D (2007) A laser sensor with multiple detectors for freeform surface digitization. Int J Adv Manuf Technol 31(11):1181–1190
7. Graebling P, Lallement A, Zhou D, Hirsch E (2002) Optical high-precision three-dimensional vision-based quality control of manufactured parts by use of synthetic images and knowledge for image-data evaluation and interpretation. Appl Opt 41(14):2627–2643
8. Prieto F, Redarce T, Lepage R, Boulanger P (2002) An automated inspection system. Int J Adv Manuf Technol 19(12):917–925
9. Bertagnolli F, Dillmann R (2003) Flexible automated process assurance through noncontact 3D measuring technology. In: Proceedings of IEEE international conference on multisensor fusion and integration for intelligent systems, vol 1, pp 27–31
10. Suh S, Lee E, Kim H, Cho J (2002) Geometric error measurement of spiral bevel gears using a virtual gear model for STEP-NC. Int J Mach Tools Manuf 42(3):335–342
11. Thomas L, Mili L, Thomas E, Shaffer C (2006) Defect detection on hardwood logs using laser scanning. Wood Fiber Sci 38(4):682–695
12. Shao W, Guo J, Shi E, Zhang T (2009) Automated inspection of sheet metal parts for manufacturing applications. In: Proceedings of IEEE international conference on industrial technology, vol 1, pp 1–6
13. Germani M, Mandorli F, Mengoni M, Raffaeli R (2010) CAD-based environment to bridge the gap between product design and tolerance control. Precis Eng 31(1):7–15
14. Rodrigues F, Gómez J, Zalama E, Perán J (2005) Automated 3D surface scanning based on CAD model. Mechatronics 15(7):837–857
15. Ravishankar S, Dutt H, Gurumoorthy B (2010) Automated inspection of aircraft parts using a modified ICP algorithm. Int J Adv Manuf Technol 46(1–4):227–236
16. Shi Q, Xi N (2008) Automated data processing for a rapid 3D surface inspection system. In: Proceedings of 2008 IEEE international conference on robotics and automation, pp 3939–3944
17. Zhang Y, Zhang Z, Zhang J (2005) Deformation visual inspection of industrial parts with image sequence. Mach Vis Appl 15(3):115–120
18. Kim J (2005) Vision-based measurement of part deformation and misalignment for deformable cylindrical peg-in-hole tasks. Proc Inst Mech Eng, C J Mech Eng Sci 219(6):589–606
19. Merkley K, Chase K, Perry E (1996) An introduction to tolerance analysis of flexible assemblies. In: Proceedings of the 1996 MSC world users conference, Newport Beach
20. Weckenmann A, Gall P, Gabbia A (2005) 3D surface coordinate inspection of formed sheet material parts using optical measurement systems and virtual distortion compensation. In: Proceedings of SPIE 8th international symposium on laser metrology, vol 5776, pp 640–647
21. Weckenmann A, Weickmann J (2006) Optical inspection of formed sheet metal parts applying fringe projection systems and virtual fixation. Metrol Sci Instrum 13(4):321–334
22. Lemeš S (2010) Validation of numerical simulations by digital scanning of 3D sheet metal objects. Ph.D. thesis, University of Ljubljana
23. Jaramillo A, Boulanger P, Prieto F (2009) On-line 3-D inspection of deformable parts using FEM trained radial basis functions. In: Proceedings of IEEE 12th international conference on computer vision, vol 1, pp 1733–1739
24. Newman T, Jain A (1995) A survey of automated visual inspection. Comput Vis Image Underst 62(2):231–262
25. Felippa C (2008) Course notes: introduction to finite element methods. Technical report, University of Colorado at Boulder, Department of Aerospace Engineering Sciences
26. Zienkiewicz O, Taylor R (2000) Finite element method: the basis, vol 1. Wiley, New York
27. Hartmann F, Katz C (2007) Structural analysis with finite elements, 2nd edn. Springer, Berlin
28. Boer A, Van der Schoot M, Bijl H (2007) Mesh deformation based on radial basis function interpolation. Comput Struct 85(11):784–795
29. Ruprecht D, Muller H (1995) Image warping with scattered data interpolation. Comput Graph Appl 15(2):37–43
30. Eck M (1991) Interpolation methods for reconstruction of 3D surfaces from sequences of planar slices. CAD Comput Graph 13(5):109–120
31. Jaramillo A, Prieto F, Boulanger P (2009) Registration of deformable models by using radial basis functions. Dyna 72(157):7–16
32. Park S, Guo X, Shin H, Qin H (2006) Surface completion for shape and appearance. Vis Comput 22(3):168–180
33. Bendels G, Schnabel R, Klein R (2006) Detecting holes in point set surfaces. J WSCG 14:89–96
34. CSI (2005) SAP2000 basic analysis reference manual. Computers and Structures, Inc, Berkeley
35. Liu G, Quek S (2003) The finite element method: a practical course. Butterworth-Heinemann, Woburn